Geophysical Journal International

Geophys. J. Int. (2013) doi: 10.1093/gji/ggt315

Geophysical Journal International Advance Access published September 3, 2013

Effective poroelastic model for one-dimensional wave propagation in periodically layered media

Asiya M. Kudarova, Karel N. van Dalen and Guy G. Drijkoningen

Section of Applied Geophysics and Petrophysics, Delft University of Technology, Stevinweg 1, 2628CN *Delft, the Netherlands. E-mail: A.Kudarova@tudelft.nl*

Accepted 2013 August 2. Received 2013 April 3; in original form 2012 October 8

SUMMARY

An effective poroelastic model is proposed that describes seismic attenuation and dispersion in periodically layered media. In this model, the layers represent mesoscopic-scale heterogeneities (larger than the grain and pore sizes but smaller than the wavelength) that can occur both in fluid and solid properties. The proposed effective medium is poroelastic, contrary to previously introduced models that lead to effective viscoelastic media. The novelty lies in the application of the pressure continuity boundary conditions instead of no-flow conditions at the outer edges of the elementary cell. The approach results in effective Biot elastic moduli and effective porosity that can be used to obtain responses of heterogeneous media in a computationally fast manner. The model is validated by the exact solution obtained with the use of Floquet's theory. Predictions of the new effective poroelastic model are more accurate than the predictions of the corresponding effective viscoelastic model when the Biot critical frequency is of the same order as the frequency of excitation, and for materials with weak frame. This is the case for media such as weak sandstones, weakly consolidated and unconsolidated sandy sediments. The reason for the improved accuracy for materials with low Biot critical frequency is the inclusion of the Biot global flow mechanism which is not accounted for in the effective viscoelastic media. At frequencies significantly below the Biot critical frequency and for well-consolidated porous rocks, the predictions of the new model are in agreement with previous solutions.

Key words: Permeability and porosity; Body waves; Seismic attenuation; Wave propagation.

1 INTRODUCTION

A lot of attention has been paid to the proper description of seismic wave attenuation in porous media over the last decades. Currently, it is widely accepted that attenuation in porous materials is associated with the presence of pore fluids and caused by a mechanism often referred to as wave-induced fluid flow. Flow of the pore fluid can occur at different spatial scales, that is, on the microscopic, mesoscopic and macroscopic scales. Generally, flow is caused by pressure gradients created by passing waves. The flow dissipates energy of the passing wave as it implies a motion of the viscous fluid relative to the solid frame of the porous material.

Wave-induced fluid flow resulting from wavelength-scale pressure gradients between peaks and troughs of a passing seismic wave is often called macroscopic or global flow as the flow takes place on the length scale of the seismic wave. In many practical situations, this mechanism is not the dominant attenuation mechanism of a seismic wave, though it is not always negligible since it depends on parameters such as permeability and porosity. For a medium containing inhomogeneities smaller than the wavelength but much larger than the typical pore size, a passing wave induces a pressure gradient on the subwavelength scale that drives a so-called mesoscopic flow. It is widely believed that it is this mechanism, the wave-induced fluid flow between mesoscopic inhomogeneities, that is the main cause of wave attenuation in the seismic frequency band (e.g. Müller & Gurevich 2005; Müller *et al.* 2010). Inhomogeneities can also be present on the scale of the pore size. In that case, passing waves induce local or microscopic flow, but its effect is often rather small for seismic waves as the mechanism becomes active only at relatively high frequencies (Pride *et al.* 2004).

In this paper, we consider media that have mesoscopic inhomogeneities. In such media the inhomogeneities can occur both in fluid (partial or patchy saturation) and in frame (e.g. double porosity) properties. The direct method to account for the presence of such inhomogeneities and its effect on attenuation is to solve the equations of poroelasticity (Biot 1956; Schanz 2009; Carcione *et al.* 2010) with spatially varying coefficients. However, this can be computationally cumbersome and time consuming, thus motivating the development of effective-medium approaches where frequency-dependent coefficients are derived and used as input for the

equations of a homogeneous effective medium. The simplest example of this approach is the homogenization of a periodically layered medium in which each layer is homogeneous and waves propagate normal to the layering. White *et al.* (1975) derived a low-frequency approximation of an effective compressional (*P*) wave modulus for such a medium by applying an oscillatory compressional test to the representative element that consists of half of the periodic cell and has undrained boundaries (i.e. no-flow conditions). This analysis showed that attenuation is quite significant when the fluid content in each of the layers is considerably different, like for the combination of water and much more compressible gas. White's result has been confirmed by other authors who came to the same effective modulus in a slightly different way. Norris (1993) derived the asymptotic approximation of the fast *P*-wave Floquet wavenumber in the context of quasi-static Biot's theory and defined the effective modulus based on that. Brajanovski *et al.* (2005) also based the effective modulus on a wavenumber but used a low-frequency approximation of the matrix propagator method. The low-frequency approximations were overcome by Vogelaar & Smeulders (2007), who solved the White's model in the context of full Biot's equations.

Dutta & Seriff (1979) showed that the geometry of heterogeneities plays a minor role on the behaviour of the media as long as the heterogeneities are much smaller than the wavelength. This justifies studies with periodic stratification, the great advantage of which is the availability of analytical expressions for the effective moduli that provide insight and that are easy to apply. Based on White's periodic model, Carcione & Picotti (2006) focused on the analysis of different heterogeneities in rock properties that led to high attenuation. They found that changes in porosity and fluid properties cause the most attenuation compared to inhomogeneities in the grain and frame moduli. Wave propagation in fractured porous media is studied by taking a limit case of White's model in which the thickness of one of the layers goes to zero and its porosity goes to one (Brajanovski *et al.* 2005; Deng *et al.* 2012). Krzikalla & Müller (2011) made an extension of the periodic model to arbitrary angles of incidence, thus accounting for shear wave attenuation as well. Carcione *et al.* (2011) used this analytical extension to validate their numerical oscillatory tests on a stack of layers from which they determined the complex stiffnesses of an effective transversely isotropic medium. They refer to this extension as Backus–White model, because it is based on White's result and the extension of the O'Doherty–Anstey formalism, and on Backus averaging applied to poroelasticity by Gelinsky & Shapiro (1997). Apparently, the periodic model of White is the starting point of many other studies on partially saturated media. Rubino *et al.* (2009) proposed an equivalent medium for a more realistic geometry of heterogeneities than in White's model, also using oscillatory compressibility (and shear) tests in the space-frequency domain. This approach is used, in particular, in studies on CO_2 monitoring (Rubino *et al.* 2011; Picotti *et al.* 2012).

The above-discussed effective media that capture the mesoscopic attenuation mechanism are in fact viscoelastic media. In all 1-D models, only one frequency-dependent elastic modulus is obtained for the considered representative element. This is a result of employing the no-flow boundary condition (undrained boundary), which implies that there is no relative fluid-to-solid motion at the outer edges of the representative element. Consequently, there is only one degree of freedom in the effective medium, which is the displacement of the frame; the effective medium thus allows for the existence of only one *P*-wave mode. Although the derivation of the effective modulus is based on the equations of poroelasticity, the obtained effective models can therefore be referred to as viscoelastic, as it was explicitly done for 2-D case by Rubino *et al.* (2009). A viscoelastic model is after all characterized by a single complex-valued frequency-dependent bulk modulus, being the counterpart of a temporal convolution operator in the time-domain stress–strain relation (e.g. Carcione 2007); a poroelastic model would require more effective parameters. Reduction of parameters and degrees of freedom in the effective medium facilitates its application and increases efficiency of computations, thus making the application of the equivalent viscoelastic media popular for studies of mesoscopic loss in porous media. Dutta & Ode (1979) noted, however, that the choice of boundary conditions at the outer edges of the representative element, as originally made by White *et al.* (1975), is not unique. Instead of the no-flow condition, the pressure continuity condition may be applied, as commonly used at the interface of two porous layers (Deresiewicz & Skalak 1963).

In this paper, we derive an effective model for the same periodic configuration as considered by White, but using the pressure continuity boundary condition that allows relative fluid-to-solid motion at the outer edges of the representative element (for which we take the full periodic cell). We show that this leads to an effective poroelastic model that has two degrees of freedom, the frame and fluid displacements, and that allows the existence of both the fast and the slow compressional waves. The choice of boundary conditions implies that flow on the wavelength scale is permitted and the effective poroelastic model thus also captures the macroscopic attenuation mechanism (next to the mesoscopic mechanism). The effect of both global and mesoscopic flow on wave propagation in layered media normal to the layering was also captured by Gelinsky *et al.* (1998), who proposed a statistical model for small fluctuations of the medium parameters and introduced an approximate solution for frequencies well below Biot critical frequency. We derive frequency-dependent effective poroelastic parameters valid for any contrast in medium parameters and for all frequencies where the effective model approach is valid. We also derive low-frequency approximations of the effective parameters. The frequency-dependent (fast) *P*-wave attenuation and transient point-source responses are compared to those predicted by the full-frequency range version of White's model (Vogelaar & Smeulders 2007) and to the analytical solution as obtained using Floquet's theory (Floquet 1883). It appears that the effective poroelastic model yields the proper *P*-wave attenuation even in situations where the macroscopic attenuation mechanism plays a significant role.

The paper is structured as follows. First, the basic equations of Biot's theory are introduced in Section 2. Then, the derivation of the effective porous medium is given (Section 3, supported by Appendices A and B). Expressions for point-source responses are derived in Section 4 (and Appendix C), and numerical results are presented in Section 5. Limitations of the effective poroelastic model are discussed in Section 6 and conclusions are given in Section 7.

2 BIOT THEORY OVERVIEW

In this section, the basic equations of Biot's theory (Biot 1956) expressed for the displacement fields in porous media are introduced. The 1-D form of the stress–strain relations reads

$$-\phi p = Qu' + Rw',$$
$$-\sigma - (1-\phi)p = Pu' + Qw'. \tag{1}$$

Here ϕ is the porosity, p is the pore fluid pressure, σ is the intergranular stress, u is the solid and w is the fluid displacements with respect to an absolute frame of reference. The prime stands for the

spatial derivative. The poroelastic coefficients P, Q, R are related to the porosity, the bulk moduli of the grains (K_s), fluid phase (K_f) and the drained matrix (K_m), as well as to the shear modulus (μ), via the following expressions:

$$P = \frac{\phi K_m + (1-\phi)K_f\,(1-\phi-K_m/K_s)}{\phi + K_f\,(1-\phi-K_m/K_s)\,/K_s} + \frac{4}{3}\mu,$$

$$Q = \frac{\phi K_f\,(1-\phi-K_m/K_s)}{\phi + K_f\,(1-\phi-K_m/K_s)\,/K_s},$$

$$R = \frac{\phi^2 K_f}{\phi + K_f\,(1-\phi-K_m/K_s)\,/K_s}. \tag{2}$$

The momentum equations read

$$-\sigma' - (1-\phi)p' = \rho_{11}\ddot{u} + \rho_{12}\ddot{w} + b*(\dot{u}-\dot{w}),$$

$$-\phi p' = \rho_{12}\ddot{u} + \rho_{22}\ddot{w} - b*(\dot{u}-\dot{w}), \tag{3}$$

where a dot stands for a time-derivative, $*$ for temporal convolution, ρ_{11}, ρ_{12} and ρ_{22} are the real-valued density terms related to the porosity, the fluid density ρ_f, the solid density ρ_s and to the tortuosity α_∞:

$$\rho_{11} = (1-\phi)\rho_s - \rho_{12},$$

$$\rho_{12} = -(\alpha_\infty - 1)\phi\rho_f,$$

$$\rho_{22} = \phi\rho_f - \rho_{12}. \tag{4}$$

In the original low-frequency Biot's theory (Biot 1956) the damping operator $b = b(t)$ is a time-independent viscous factor $b_0 = \eta\phi^2/k_0$, where η is the viscosity of the fluid, and k_0 is permeability. With the adoption of the correction to this factor to account for dynamic effects (Johnson *et al.* 1987) the viscodynamic operator $\hat{b}$ in the frequency domain reads:

$$\hat{b} = b_0\sqrt{1 + \mathrm{i}\frac{\omega}{2\omega_B}M}, \quad \mathrm{Re}(\hat{b}) > 0 \quad \text{for all} \quad \omega. \tag{5}$$

Here M is the parameter that depends on the geometry of the pores, permeability and porosity. Following Johnson *et al.* (1987), we will assume $M = 1$ throughout the paper. $\omega_B = \phi\eta/(k_0\alpha_\infty\rho_f)$ is the Biot critical frequency. A hat above a quantity stands for frequency dependence. The transition to the frequency domain is carried out by a Fourier transform defined as

$$\hat{f}(\omega) = \int_{-\infty}^{\infty} \exp(-\mathrm{i}\omega t) f(t)\,\mathrm{d}t. \tag{6}$$

The transition back to the time domain is carried out by applying the inverse Fourier transform

$$f(t) = \frac{1}{2\pi}\int_{-\infty}^{\infty} \exp(\mathrm{i}\omega t)\hat{f}(\omega)\,\mathrm{d}\omega. \tag{7}$$

The combination of the stress–strain relations (1) and the equations of motion (3) leads to a set of equations in terms of the fluid (u) and solid (w) particle displacements. These equations are solved in the frequency domain via seeking a solution in the form $\hat{u} = \hat{A}\exp(\mathrm{i}kx)$, $\hat{w} = \hat{B}\exp(\mathrm{i}kx)$. Substitution of these expressions leads to a system of linear homogeneous equations for the amplitudes $\hat{A}$, $\hat{B}$, which has a non-trivial solution when the determinant of the system is zero

$$(PR - Q^2) - (P\hat{\rho}_{22} + R\hat{\rho}_{11} - 2Q\hat{\rho}_{12})\frac{k^2}{\omega^2} + \left(\hat{\rho}_{11}\hat{\rho}_{22} - \hat{\rho}_{12}{}^2\right)\frac{k^4}{\omega^4} = 0. \tag{8}$$

Here frequency-dependent density terms are defined as

$$\hat{\rho}_{11} = \rho_{11} - \mathrm{i}\hat{b}/\omega,$$

$$\hat{\rho}_{12} = \rho_{12} + \mathrm{i}\hat{b}/\omega,$$

$$\hat{\rho}_{22} = \rho_{22} - \mathrm{i}\hat{b}/\omega. \tag{9}$$

The dispersion eq. (8) has four roots $\pm k_{P1}$, $\pm k_{P2}$ that correspond to the wavenumbers of the up- and downgoing fast and slow P-waves. The fluid-to-solid amplitude ratios for both waves are

$$\hat{\beta}_{P1,P2} = -\frac{Pk^2_{P1,P2} - \hat{\rho}_{11}\omega^2}{Qk^2_{P1,P2} - \hat{\rho}_{12}\omega^2}. \tag{10}$$

Thus, for arbitrary excitation the displacement fields read

$$\hat{u}(x) = \hat{A}_1\mathrm{e}^{\mathrm{i}k_{P1}x} + \hat{A}_2\mathrm{e}^{\mathrm{i}k_{P2}x} + \hat{A}_3\mathrm{e}^{-\mathrm{i}k_{P1}x} + \hat{A}_4\mathrm{e}^{-\mathrm{i}k_{P2}x},$$
$$\hat{w}(x) = \hat{\beta}_{P1}\left(\hat{A}_1\mathrm{e}^{\mathrm{i}k_{P1}x} + \hat{A}_3\mathrm{e}^{-\mathrm{i}k_{P1}x}\right) + \hat{\beta}_{P2}\left(\hat{A}_2\mathrm{e}^{\mathrm{i}k_{P2}x} + \hat{A}_4\mathrm{e}^{-\mathrm{i}k_{P2}x}\right). \tag{11}$$

The amplitudes $\hat{A}_1$ to $\hat{A}_4$ are determined by the excitation and boundary conditions. These expressions will be used in further derivations.

3 EFFECTIVE POROELASTIC MODEL FOR PERIODIC LAYERING

In this section, effective frequency-dependent poroelastic parameters are derived to describe wave propagation in periodically stratified media normal to the stratification. The periodic medium and its elementary cell are depicted in Fig. 1. The thicknesses of the layers are denoted by l_I and l_{II}, and $L = l_I + l_{II}$ is the period of the system. Each of the layers I and II is homogeneous and is described by Biot's equations introduced in the previous section, and has its own set of material properties contained in the coefficients (2), (4) and (5).

Since we consider the period L much smaller than the wavelength, it is reasonable to regard some elementary cell as a representative volume of the homogeneous effective medium. Then the elastic moduli can be determined from oscillatory compressional-stress tests. A similar approach has been used by White *et al.* (1975), but with a different choice of boundary conditions; they chose a representative elementary cell that consists of the halves of the layers and applied the total stress continuity and no-flow conditions at the outer edges of the elementary cell. Here, the full periodic cell is chosen and an oscillatory pressure p is applied together with an oscillatory intergranular stress σ at the outer edges of the elementary cell, as depicted in Fig. 1 (right-hand panel). We emphasize that, with this choice (suggested by Dutta & Ode 1979), no kinematic condition restricting the flow across the outer edges of the cell is applied; two phases, solid and fluid displacements, remain in the effective medium, while the no-flow condition allows for only one phase in the effective medium.

The solutions of Biot's equations in each of the layers consist of up- and downgoing plane waves (as in eq. 11)

$$\hat{u}_{I,II} = \sum_{i=1}^{4} \hat{A}_i^{I,II}\exp\left(\mathrm{i}k_i^{I,II}x\right),$$

$$\hat{w}_{I,II} = \sum_{i=1}^{4} \hat{\beta}_i^{I,II}\hat{A}_i^{I,II}\exp\left(\mathrm{i}k_i^{I,II}x\right). \tag{12}$$

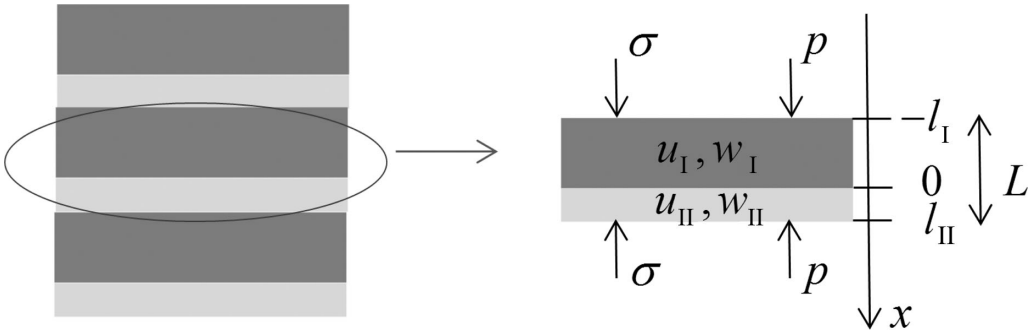

Figure 1. Left-hand panel: periodically layered medium; right-hand panel: its elementary cell.

Throughout the paper the indices and superscripts I and II refer to the properties of the layers I and II, respectively. The wavenumbers $k_i^{\mathrm{I,II}}$ for each of the layers are found as the roots of the corresponding dispersion eqs (8) and the fluid-to-solid amplitude ratios $\hat{\beta}_i^{\mathrm{I,II}}$ are found according to relations (10). In order to find the unknown amplitudes $\hat{A}_i^{\mathrm{I,II}}$ a system of eight linear algebraic equations has to be solved that follow from the eight boundary conditions

$$\{\hat{u}_{\mathrm{I}}, \hat{\zeta}_{\mathrm{I}}, \hat{\sigma}_{\mathrm{I}}, \hat{p}_{\mathrm{I}}\}|_{x=0} = \{\hat{u}_{\mathrm{II}}, \hat{\zeta}_{\mathrm{II}}, \hat{\sigma}_{\mathrm{II}}, \hat{p}_{\mathrm{II}}\}|_{x=0},$$

$$\hat{p}_{\mathrm{I}}(-l_{\mathrm{I}}) = \hat{p}, \qquad \hat{p}_{\mathrm{II}}(l_{\mathrm{II}}) = \hat{p},$$

$$\hat{\sigma}_{\mathrm{I}}(l_{\mathrm{I}}) = \hat{\sigma}, \qquad \hat{\sigma}_{\mathrm{II}}(l_{\mathrm{II}}) = \hat{\sigma}. \tag{13}$$

Here, the first four boundary conditions assume the continuity of intergranular stress, pore pressure, solid particle displacement and fluid displacement relative to the matrix $\hat{\zeta} = \phi(\hat{w} - \hat{u})$ at the interface between the layers I and II (following Deresiewicz & Skalak 1963). The latter four conditions express the excitation at the outer edges; they are thus different from those applied by White *et al.* (1975) and Vogelaar & Smeulders (2007). The coefficients of the linear system of equations are written out explicitly in Appendix A.

As mentioned before, the elementary cell is regarded as a representative volume of the homogenized effective medium. Thus, the strains of the elementary cell

$$\hat{u}' = \frac{\hat{u}_{\mathrm{II}}(l_{\mathrm{II}}) - \hat{u}_{\mathrm{I}}(l_{\mathrm{I}})}{L}, \quad \hat{w}' = \frac{\hat{w}_{\mathrm{II}}(l_{\mathrm{II}}) - \hat{w}_{\mathrm{I}}(l_{\mathrm{I}})}{L} \tag{14}$$

can be regarded as the strains of the effective medium. They are related to the intergranular stress and pore pressure according to Biot's stress–strain relations (1)

$$\begin{bmatrix} \hat{u}'_e \\ \hat{w}'_e \end{bmatrix} = \mathbf{E}_e^{-1} \begin{bmatrix} \hat{\sigma} \\ \hat{p} \end{bmatrix},$$

$$\mathbf{E}_e = \frac{1}{\hat{\phi}_e} \begin{bmatrix} \hat{Q}_e(1-\hat{\phi}_e) - \hat{\phi}_e \hat{P}_e & \hat{R}_e - \hat{\phi}_e(\hat{Q}_e + \hat{R}_e) \\ -\hat{Q}_e & -\hat{R}_e \end{bmatrix}. \tag{15}$$

Substitution of the amplitudes $\hat{A}_i^{\mathrm{I,II}}$, which are found after solving the system of equations from Appendix A, into eqs (12), and then substitution of the result into (14), provides the following relations:

$$\hat{u}' = \alpha_1 \hat{\sigma} + \alpha_2 \hat{p},$$

$$\hat{w}' = \alpha_3 \hat{\sigma} + \alpha_4 \hat{p}. \tag{16}$$

Here α_1 to α_4 are frequency-dependent complex-valued coefficients. In order to derive the effective Biot coefficients, eqs (15) and (16) should be compared. This leads to a system of four non-linear algebraic equations, the solution of which is

$$\hat{P}_e = -\frac{-\alpha_3\alpha_2 - \alpha_4\alpha_3 + \alpha_4\alpha_1 + {\alpha_3}^2}{{\alpha_3}^2\alpha_2 - \alpha_3\alpha_1\alpha_2 - \alpha_4\alpha_1\alpha_3 + \alpha_4{\alpha_1}^2},$$

$$\hat{Q}_e = \frac{\alpha_3(\alpha_1 - \alpha_2)}{{\alpha_3}^2\alpha_2 - \alpha_3\alpha_1\alpha_2 - \alpha_4\alpha_1\alpha_3 + \alpha_4{\alpha_1}^2},$$

$$\hat{R}_e = -\frac{\alpha_1(\alpha_1 - \alpha_2)}{{\alpha_3}^2\alpha_2 - \alpha_3\alpha_1\alpha_2 - \alpha_4\alpha_1\alpha_3 + \alpha_4{\alpha_1}^2},$$

$$\hat{\phi}_e = \frac{\alpha_1 - \alpha_2}{\alpha_1 - \alpha_3}. \tag{17}$$

These coefficients are the effective complex-valued frequency-dependent elastic moduli and porosity of the effective poroelastic medium.

In the low-frequency regime, all effective models that capture the mesoscopic attenuation mechanism predict similar behaviour of the inverse quality factor Q^{-1} of the fast compressional wave (Pride *et al.* 2003). In order to validate the effective coefficients (that are combined in Q^{-1}) in the current effective poroelastic model, we derive low-frequency analytical expressions using a perturbation method described in Appendix C. The terms of the expansion

$$\hat{\Phi}_e = \Phi_0 + \omega\Phi_1 + \omega^2\Phi_2 + \mathcal{O}(\omega^3) \tag{18}$$

can be found for each of the effective coefficients (17). The matrix $\mathbf{E}$ (eq. 15) containing the zeroth-order terms turns out to be a harmonic average of the matrices for each of the layers, exactly like a single Young's modulus for an elastic solid (also known as Wood's law):

$$\mathbf{E}_0^{-1} = \frac{l_{\mathrm{I}}}{L}\mathbf{E}_{\mathrm{I}}^{-1} + \frac{l_{\mathrm{II}}}{L}\mathbf{E}_{\mathrm{II}}^{-1}. \tag{19}$$

The analytical expressions for the first-order terms are quite big; they depend on the properties of both layers, including the viscous terms. Rather simple expressions can be obtained in the specific case of small inclusions, that is, when $l_{\mathrm{II}} \ll l_{\mathrm{I}}$, using Taylor series in l_{II}. An expansion of the Gassmann modulus $\hat{H}_e = \hat{P}_e + 2\hat{Q}_e + \hat{R}_e$ around $\omega = 0$ reads:

$$\hat{H}_e = H_0 + \mathrm{i}\chi b_0^{\mathrm{I}} l_{\mathrm{II}}\omega. \tag{20}$$

Here, $H_0 = P_0 + 2Q_0 + R_0$, $b_0^{\mathrm{I}} = (\eta\phi^2/k_0)^{\mathrm{I}}$ is the Biot damping factor of the first layer, and the coefficient χ depends on elastic moduli and porosities of the layers and is not presented here explicitly because of its size.

The theory of Biot predicts the low-frequency attenuation of the fast compressional wave Q^{-1} to be proportional to permeability k_0 (Berryman 1986). However, in media with mesoscopic heterogeneities the situation is different: the attenuation is inversely

proportional to the permeability (Pride *et al.* 2003); this is confirmed for the current effective poroelastic model

$$Q^{-1} = 2\left|\frac{\mathrm{Im}(\hat{H}_e)}{\mathrm{Re}(\hat{H}_e)}\right| = \frac{2\chi\omega\eta\phi^2 l_{\mathrm{II}}}{H_0 k_0}. \tag{21}$$

Here, for reasons of comparison Q^{-1} is defined as in Pride *et al.* (2004) for their patchy saturation model; in the remainder of this paper, a slightly different definition of Q^{-1} is adopted.

4 CONFIGURATION AND DYNAMIC RESPONSES

The dynamic response predicted by the current effective poroelastic model is validated by an exact solution (Floquet's theory, Appendix C) and compared with the response predicted by the effective viscoelastic model proposed by Vogelaar & Smeulders (2007); see next section. In this section, the specific configuration and excitation are given, as well as the derivation of the dynamic responses for different models.

4.1 Configuration

The configuration chosen for the simulations of wave propagation in different models is the typical case of partial saturation; it has been used in numerous studies, starting from White *et al.* (1975). Two different fluids fully saturate the poroelastic solid with the periodic zones in x-direction, as depicted in Fig. 2(a). Fig. 2(b) depicts the effective homogenized medium that is described either with one single viscoelastic equation, or with the single set of Biot's poroelastic equations, both with the effective coefficients. The saturations of the fluids are $s_{\mathrm{I}} = l_{\mathrm{I}}/L$, $s_{\mathrm{II}} = l_{\mathrm{II}}/L$. The dry rock properties are the same for both layers, and they do not depend on depth x. This simple configuration allows to account for the effects of fluid flow specifically.

At the top interface $x = 0$ a stress as a function of time is applied. The pore pressure is assumed to be zero at $x = 0$ (free surface). Then, the boundary conditions at the top interface for the exact solution and for the effective poroelastic model read

$$-\sigma|_{x=0} = f(t), \quad p|_{x=0} = 0. \tag{22}$$

For the viscoelastic model, there is only one boundary condition at the top interface, namely, the continuity of the solid stress τ

$$\tau|_{x=0} = f(t). \tag{23}$$

As source function, the Ricker wavelet is chosen

$$f(t) = f_0\left[1 - 2\pi^2 f_{\mathrm{R}}^2 (t - t_0)^2\right]\exp\left[-\pi^2 f_{\mathrm{R}}^2 (t - t_0)^2\right]. \tag{24}$$

Here, f_0 is a constant scaling coefficient with the dimension of stress (Pa), f_{R} is the central frequency of the wavelet and t_0 is an arbitrary time-shift chosen such that the non-zero part of the wavelet lies within the positive domain $t > 0$; only the components that are infinitely small are left in the domain $t < 0$. The dynamic responses of the media are compared far away from the source (in terms of wavelengths) in order to capture the attenuation effects, at a distance x_r below the source.

4.2 Exact solution

The exact solution for the periodically layered half-space is obtained with the use of Floquet's theory (Floquet 1883). For elastic composites, the procedure has been implemented by Braga & Hermann (1992). For periodic poroelastic layering, Floquet's theory has been applied by Norris (1993), but the full solution is not present in that paper, as the author worked with low frequencies and only with the fast P-wave mode. In most cases of interest, the low-frequency solution suffices within the seismic frequency band. However, this is not always the case. In particular, when the Biot critical frequency is relatively small so that the assumption $\omega \ll \omega_{\mathrm{B}}$ is violated in the seismic frequency band, the full solution is required. Examples are shown in the next section. The procedure of obtaining the exact solution, which contains two modes, in the frequency domain is given in Appendix C. In the examples provided in the next section, this solution is used for validating the effective media at frequencies well below the stop and pass bands typical for periodic structures, because the effective media cannot be applied at higher frequencies where the assumption of the wavelength being much larger than the period is violated. Nevertheless, the exact solution is valid for any frequency.

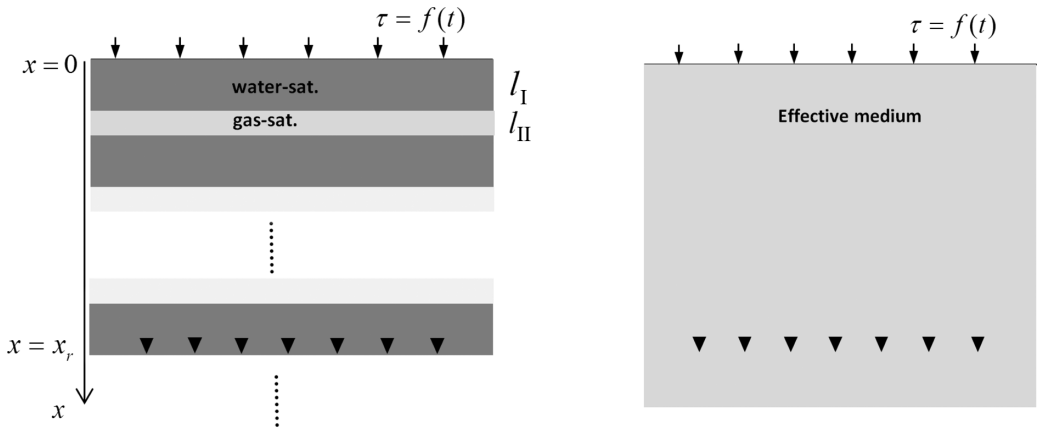

Figure 2. Geometry of a periodically stratified poroelastic solid (a) and its homogenized analogue (b).

Table 1. Sets of material properties chosen for simulations.

Parameter	Notation	Units	Rock	Sand 1	Sand 2	Sand 3	Sand 4
Density of solid grains	ρ_s	kg m^{-3}	2650	2650	2650	2690	2650
Bulk modulus of solid grains	K_s	GPa	40	36	36	32	40
Bulk modulus of frame	K_m	GPa	12.7	0.22	0.044	0.044	0.2
Porosity	ϕ	–	0.15	0.35	0.4	0.38	0.38
Permeability	k_0	m^2	10^{-13}	10^{-10}	10^{-10}	2.5×10^{-11}	6.49×10^{-12}
Shear modulus	μ	GPa	20.3	0.1	0.026	0.03	0.12
Tortuosity	α_∞	–	1	1.25	1.25	1.35	1.25
Biot critical frequency (100 per cent water saturation)	$\frac{\omega_B}{2\pi}$	Hz	2.4×10^5	446	509	1792	7514

4.3 Effective poroelastic model solution

The system of linear equations from Appendix A is solved numerically (with the application of the standard function of International Mathematics and Statistics Library for Fortran) for each frequency. Then, the effective coefficients (17) are obtained. In order to find the response of the effective poroelastic model Biot's equations of motion are solved first in the frequency domain using the derived effective coefficients. Then the response in time domain is found by applying the inverse Fourier transform (7). The effective density of the fluid is taken as an arithmetic average: $\rho_f^e = s_I \rho_f^I + s_{II} \rho_f^{II}$. The effective frequency-dependent density terms (9) are also determined from arithmetic averages

$$\hat{\rho}_{ij} = s_I \hat{\rho}_{ij}^I + s_{II} \hat{\rho}_{ij}^{II}. \tag{25}$$

This is consistent with taking $(\eta/\hat{k}_0)_e = s_I(\eta/\hat{k}_0)_I + s_{II}(\eta/\hat{k}_0)_{II}$ as the effective inverse fluid mobility that can be derived from Darcy's law applied to the elementary cell in Fig. 1 (*cf.* Schoemaker 2011). Here, for the individual layers, the dynamic permeability $\hat{k}_0$ is defined as (Johnson *et al.* 1987)

$$\hat{k}_0 = k_0 \left(\sqrt{1 + \mathrm{i} \frac{\omega}{2\omega_B} M} + \mathrm{i} \frac{\omega}{\omega_B} \right)^{-1}. \tag{26}$$

We note that, in the limiting case of a homogeneous medium, this dynamic permeability results in the frequency-dependent damping term $\hat{b}$ given in (5), and thus in the density terms $\hat{\rho}_{ij}$ specified in (9).

The solution of Biot's equations with the effective coefficients is thus found in the form (11). The amplitudes of the upgoing waves are zero due to the fact that there are no sources at infinity, and all the field variables should go to zero at infinity for a system with viscous damping (on account of the radiation condition). Thus, only two amplitudes of the exponential terms $\exp(-\mathrm{i}k_{P1}^e x)$ and $\exp(-\mathrm{i}k_{P2}^e x)$, where $k_{P1,P2}^e$ are the effective fast and slow compressional wavenumbers, respectively, and $\mathrm{Im}(k_{P1,P2}^e) < 0$, are to be found. The two boundary conditions (22) determine the system of linear equations with the unknown amplitudes $\hat{A}_3$ and $\hat{A}_4$

$$\begin{aligned} &\left(\hat{Q}_e + \hat{R}_e \hat{\beta}_{P1}^e\right) k_{P1}^e \hat{A}_3 + \left(\hat{Q}_e + \hat{R}_e \hat{\beta}_{P2}^e\right) k_{P2}^e \hat{A}_4 = 0, \\ &\mathrm{i}\left(\hat{P}_e + \hat{Q}_e \hat{\beta}_{P1}^e\right) k_{P1}^e \hat{A}_3 + \mathrm{i}\left(\hat{P}_e + \hat{Q}_e \hat{\beta}_{P2}^e\right) k_{P2}^e \hat{A}_4 = \hat{f}(\omega), \end{aligned} \tag{27}$$

where $\hat{f}(\omega)$ is the Fourier transform of the wavelet (24). $\hat{A}_3$ and $\hat{A}_4$ are easily found from this system of equations:

$$\begin{aligned} \hat{A}_3 &= \frac{\mathrm{i}\left(\hat{Q}_e + \hat{R}_e \hat{\beta}_{P2}^e\right) \hat{f}}{k_{P1}^e \left(\hat{P}_e \hat{R}_e - \hat{Q}_e^2\right)\left(\hat{\beta}_{P1}^e - \hat{\beta}_{P2}^e\right)} \\ \hat{A}_4 &= -\frac{\mathrm{i}\left(\hat{Q}_e + \hat{R}_e \hat{\beta}_{P1}^e\right) \hat{f}}{k_{P2}^e \left(\hat{P}_e \hat{R}_e - \hat{Q}_e^2\right)\left(\hat{\beta}_{P1}^e - \hat{\beta}_{P2}^e\right)}. \end{aligned} \tag{28}$$

4.4 Effective viscoelastic model solution

Following Vogelaar & Smeulders (2007), the effective viscoelastic model defines the effective frequency-dependent bulk modulus $\hat{H}$. The wave propagation in the effective medium is described with the viscoelastic wave equation

$$-\rho\omega^2 \hat{u} - \hat{H}\hat{u}'' = 0, \tag{29}$$

where the effective density ρ is an arithmetic average of the fluid and solid densities $\rho_f^{I,II}$ and $\rho_s^{I,II}$ in each of the layers, defined as

$$\rho = s_I \left[(1-\phi)\rho_s^I + \phi\rho_f^I\right] + s_{II}\left[(1-\phi)\rho_s^{II} + \phi\rho_f^{II}\right]. \tag{30}$$

The solution of the eq. (29) in the frequency domain can be found in the same way as for the poroelastic model. Only a downgoing wave is allowed due to the same radiation condition

$$\hat{u} = \hat{A}\exp(-\mathrm{i}kx), \qquad k = \omega\sqrt{\rho/\hat{H}}, \quad \mathrm{Im}(k) < 0. \tag{31}$$

The excitation is the same as in the poroelastic model. The amplitude $\hat{A}$ is found from the boundary condition (23) in the frequency domain

$$\hat{\tau}|_{x=0} = \hat{f}(\omega) = \hat{H}\hat{u}'|_{x=0} = -\hat{H}\hat{A}\mathrm{i}k \quad \Rightarrow \quad \hat{A} = \frac{\mathrm{i}\hat{f}(\omega)}{\hat{H}k}. \tag{32}$$

5 RESULTS

In this section, the results of simulations and comparison of the dynamic responses are presented. The sets of chosen material properties for the solid phase are given in Table 1. They represent a typical porous rock with stiff frame and high Biot critical frequency (Rock), and a number of sands ranging from unconsolidated to weakly consolidated with much lower Biot critical frequency for which we expect different behaviour of the effective poroelastic and viscoelastic models. The references for each of the sets are given in the text below. Pore fluid and gas properties are listed in Table 2. They are taken from Gelinsky & Shapiro (1997). The following parameters are chosen for the Ricker wavelet (eq. 24): $t_0 = 0.022$ s, $f_R = 50$ Hz, $f_0 = 1$ GPa. The position of the receiver is chosen at a distance $x_r = 10^3 \cdot L$ below the source.

The first set of material properties from Table 1 (Rock) is taken from Gelinsky & Shapiro (1997). It is a porous rock with high

Table 2. Mechanical properties of the sample pore fluids: water and gas.

Parameter	Notation	Units	Water	Gas
Density	ρ_f	kg m^{-3}	1000	140
Bulk modulus	K_f	GPa	2.25	0.056
Viscosity	η	Pa s	0.001	0.00022

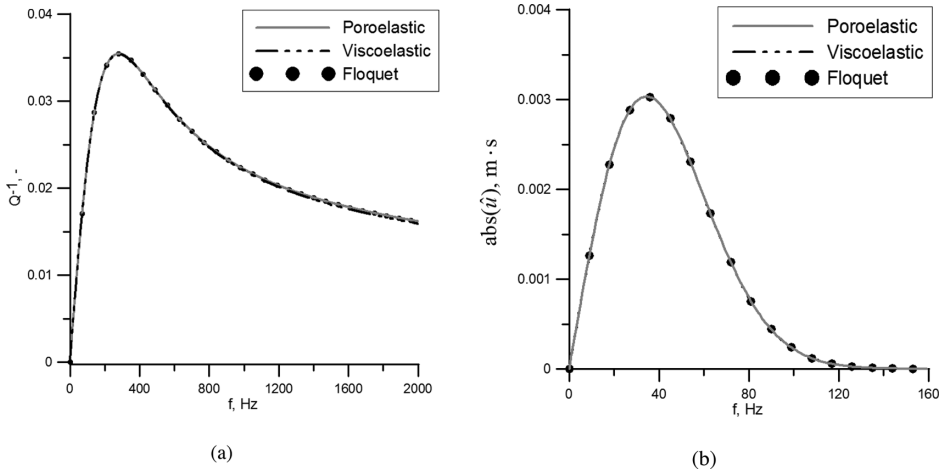

Figure 3. Inverse quality factor Q^{-1} (a) and frequency spectrum (b). Rock, $L = 0.1$ m, gas saturation 10 per cent. On both plots all three lines coincide.

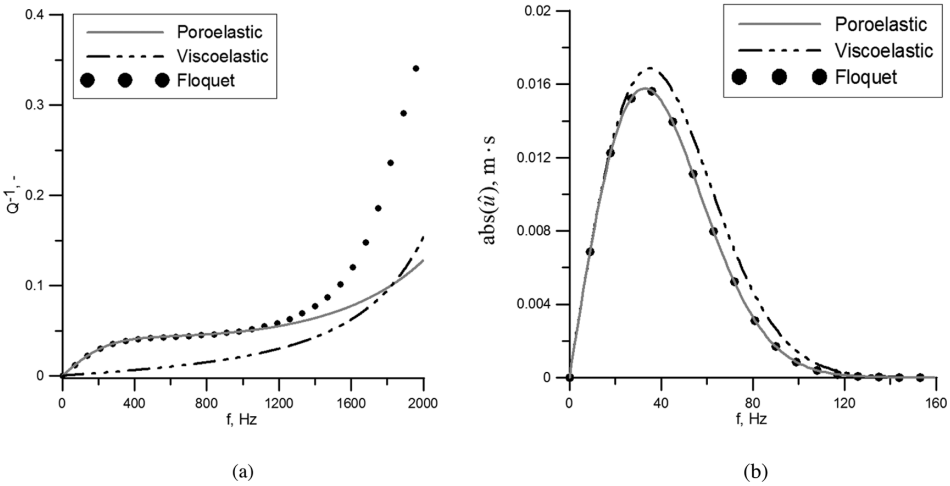

Figure 4. Inverse quality factor Q^{-1} (a) and frequency spectrum (b). Sand 1, $L = 0.1$ m, gas saturation 10 per cent.

Biot critical frequency (well outside the seismic range) and well consolidated. For a gas saturation of 10 per cent, the inverse quality factor $Q^{-1} = 2|\mathrm{Im}(k^e_{P1})/\mathrm{Re}(k^e_{P1})|$ (where k^e_{P1} is the fast P-wave wavenumber) versus frequency $f = \omega/(2\pi)$ is depicted in Fig. 3(a). As one can see from the plot, the responses of the effective poro- and viscoelastic models (grey solid line and black dotted line, respectively) and the exact solution (black circles) almost coincide. In agreement with this prediction, we find that the magnitudes of the responses in the frequency domain (the absolute values of the solid particle displacement) of all three models coincide (Fig. 3b).

Sand 1 from Table 1 is an example of coarse sand. It has much higher permeability than Rock and, as a consequence, much lower value of the Biot critical frequency that is of the same order as the frequency of excitation. The set of physical properties is taken from Turgut & Yamamoto (1990). Because of the lack of data of tortuosity for this sand, it is assumed to be the same as for Sand 2. As one can see in Fig. 4, the agreement between the attenuations and responses predicted by the models is violated for Sand 1. There is a large difference between the models in the predicted attenuations (Fig. 4a). The poroelastic model predicts practically the same attenuation as the exact solution over a broad frequency range; deviations occur with increasing frequency, but that is expected because the associated wavelengths get smaller so that the effective model becomes inappropriate. However, the viscoelastic model significantly underestimates the attenuation at all frequencies where the effective-model approach is supposed to be valid. As a result, the magnitude of the response of the viscoelastic model differs from that of the exact solution and the poroelastic model (Fig. 4b), while the latter two coincide. The low value of Biot critical frequency in case of Sand 1 implies that the frequency dependence of the viscodynamic operator $\hat{b}$ that is contained in the effective densities (eq. 25) (*cf.* eq. 9 for a homogeneous medium) starts to play a role, and that the macroscopic attenuation mechanism gives a non-negligible contribution to the damping of the propagating wave, which is not captured by the effective viscoelastic model. The latter model only captures the mesoscopic mechanism and does not allow fluid flow on the macroscopic scale due to the no-flow boundary conditions at the outer edges of the representative elementary cell.

One can note that different frequency ranges are shown in the plots of the attenuations and responses. The frequency range in the plots of the responses corresponds to the width of the frequency spectrum of the excitation wavelet. Relatively low frequencies have been chosen for the excitation wavelet to demonstrate realistic responses of the different models at a certain depth (100 m). In principle, the difference between the predictions of the models

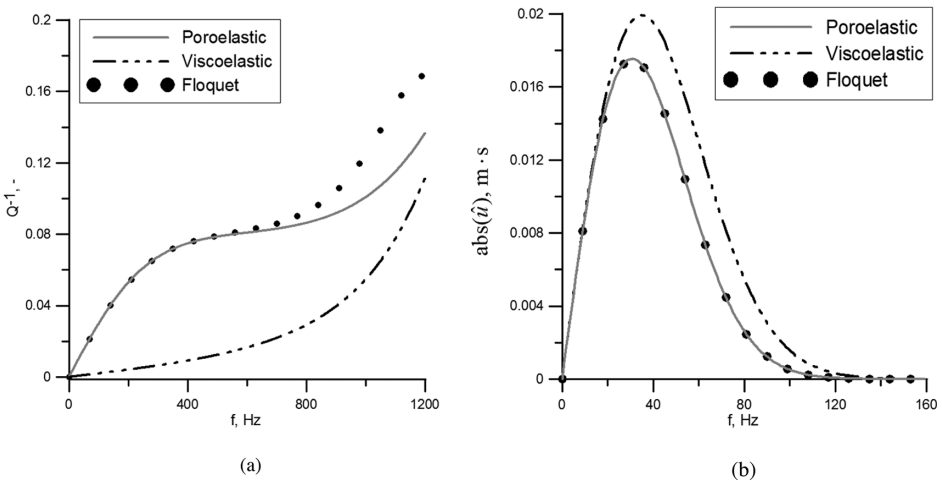

(a) (b)

Figure 5. Inverse quality factor Q^{-1} (a) and frequency spectrum (b). Sand 2, $L = 0.1$ m, gas saturation 10 per cent.

varies with frequency, ratio of inhomogeneities (gas saturation) and distance from the source. The attenuation plots show the difference between the models at a broader frequency range and provide an insight into possible deviations in the magnitudes of the responses at higher frequencies. In most of the plots (Figs 4a, 5a, 7a, 8a and 9b) the predictions of attenuations by the effective poroelastic model start to deviate from the predictions of the exact solution at higher frequencies. This is due to the violation of the effective medium approach: the wavelength of a propagating wave becomes shorter (compared to the period of the system).

The next example (Sand 2 from Table 1) is also a high-permeable material with low Biot critical frequency which has weaker frame than Sand 1. It is an unconsolidated sand sediment. This set of material properties is taken from Williams (2001), keeping only real parts of the bulk moduli. The inverse quality factor for gas saturation 10 per cent is depicted in Fig. 5(a). The poroelastic model predicts the same attenuation as the exact solution at all frequencies of interest for the current configuration (where the effective medium approach is valid). The magnitudes of the responses for different saturations are depicted in Figs 5(b) and 6(a)–(d). As one can note, the difference in the magnitudes of the responses increases with the increase of gas saturation. Again, the viscoelastic model underestimates attenuation for all gas saturations, while the poroelastic model is in agreement with the exact solution. The viscoelastic model underestimates the attenuation by almost a factor two for high gas saturation (Fig. 6d).

Sand 3 has been chosen as an example of a weakly consolidated material with lower permeability and higher Biot critical frequency than in the previous examples of sands. This set of material properties has been taken from Hefner & Jackson (2010). The parameters of this sand are referred to as SAX99 in the mentioned paper; they were obtained during the sediment acoustics experiment in 1999. The predicted attenuations for gas saturations of 10 and 90 per cent are depicted in Figs 7(a) and 8(a), respectively. As in the previous examples, the poroelastic model predicts practically the same attenuation as the exact solution, and the viscoelastic model significantly underestimates the attenuation. The difference in the magnitude of the responses for gas saturation 10 per cent (Fig. 7b) is not as large as for Sand 2 (Fig. 5b), but it also increases with the increase of gas saturation (Fig. 8b).

As can be concluded based on the examples shown above, the differences in predictions of the models become less pronounced with the decrease of permeability (increase of Biot critical frequency; *cf.* Sands 2 and 3) and increase of bulk and shear moduli of the frame (for materials with equal permeability, *cf.* examples Sand 1 and Sand 2). This observation is confirmed by the results for Sand 4 (Fig. 9) that has even lower permeability than Sand 3 and stiffer frame. This set of material properties has been taken from Chotiros (1995), where it is referred to as Ottawa sand. As in the previous examples, the difference between the models is more pronounced for higher gas saturations. The inverse quality factor for saturation 10 per cent is depicted in Fig. 9(a). The poroelastic model and the exact solution are in agreement; the viscoelastic model slightly underestimates the attenuation with increasing frequency. However, this would hardly affect the magnitude of the responses for the chosen configuration (the corresponding plot is left out). The difference between all three models is significant for a gas saturation of 90 per cent (Fig. 9b). At low frequencies the poroelastic model still gives the same result as the exact solution, while the viscoelastic model predicts less attenuation. At higher frequencies, where the effective medium approach is violated, all solutions give different results. Still, the prediction of the poroelastic model is closer to the exact solution than that of the viscoelastic model. The response in the frequency domain for a gas saturation of 90 per cent is depicted in Fig. 9(c). A higher central frequency (200 Hz) of the Ricker wavelet is taken for this example in order to distinguish differences between the responses. As can be expected based on the attenuation plot, the viscoelastic model overestimates the magnitude of the response. The results for Sand 4 show that the viscoelastic model can still be less accurate for materials with Biot critical frequency much higher than the frequency of excitation, but this inaccuracy has much less pronounced effect on the magnitude of the responses in the frequency range of interest for seismic applications. For materials with much higher Biot critical frequency and stiffer frame, like Rock from the first example, both effective viscoelastic and poroelastic models are in agreement with each other and the exact solution.

6 DISCUSSION

The use of an effective medium requires that the involved wavelengths are much larger than the period L of the medium. The weak point of the current effective poroelastic model is that the wavelength of the slow P-wave can be very small (i.e. of the order of the

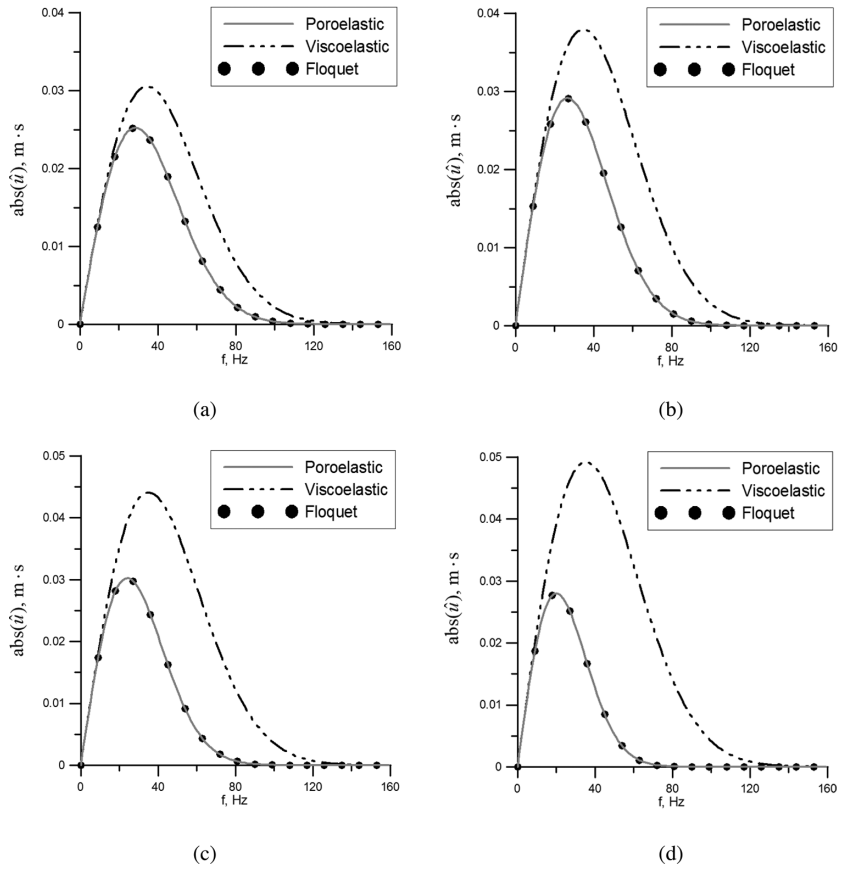

Figure 6. Frequency spectrum $|\hat{u}|$ for gas saturations (a) 30 per cent; (b) 50 per cent; (c) 70 per cent; (d) 90 per cent. Sand 2, $L = 0.1$ m.

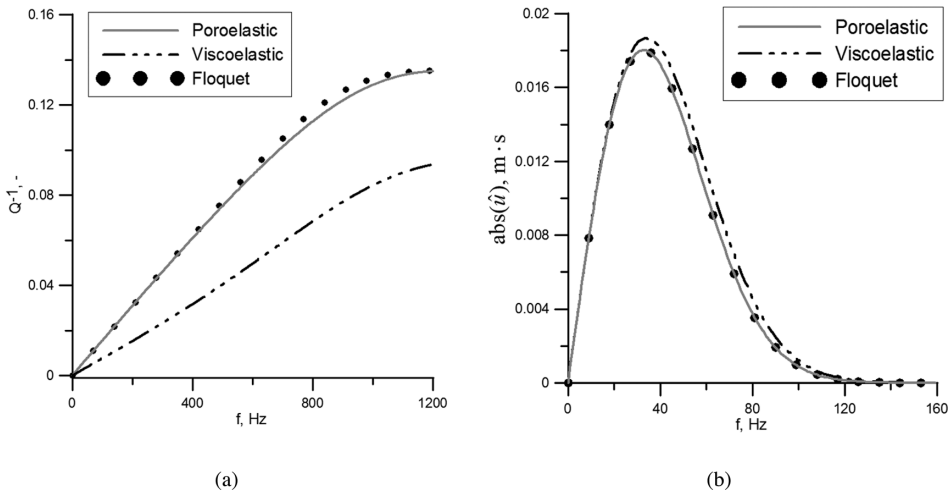

Figure 7. Inverse quality factor Q^{-1} (a) and frequency spectrum (b). Sand 3, $L = 0.1$ m, gas saturation 10 per cent.

period of the system or even smaller), which thus violates the requirement. However, this inconsistency hardly affects the response of the effective poroelastic medium as the contribution of the slow *P*-wave to the total response is generally very small at seismic frequencies. Possibly superior approaches of homogenization that circumvent the inconsistency exist, but the present analysis shows that the choice of the pressure continuity condition in (13) at the edge of the representative elementary cell, rather than the no-flow condition, can be important for the behaviour of the effective model. The no-flow boundary condition is in fact quite restrictive as it excludes the macroscopic attenuation mechanism from the effective model (see also Sections 1 and 5). This restriction is thus circumvented by applying the pressure continuity condition suggested by Dutta & Ode (1979), and this is particularly important when dealing with high permeable materials such as weak sandstones, unconsolidated and weakly consolidated sandy sediments. The effective poroelastic model, or the exact solution, should be used when the signal frequency is of the same order as the Biot critical frequency. The predictions of the effective viscoelastic model are also less accurate for materials with weak frame.

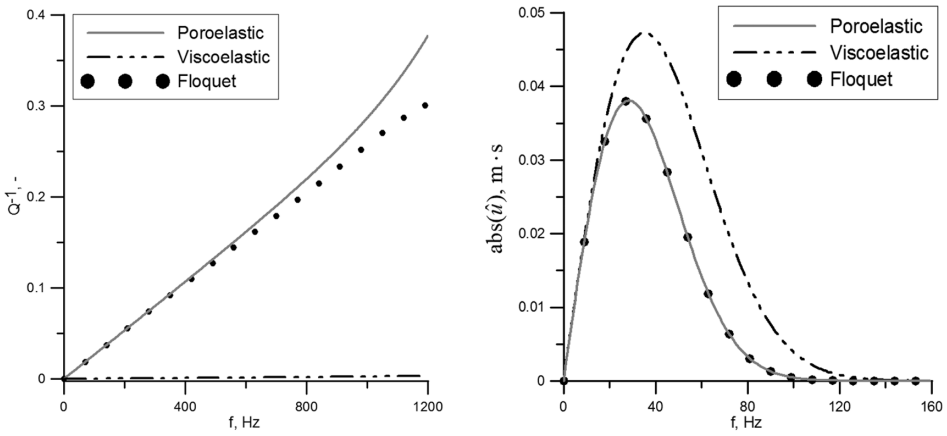

Figure 8. Inverse quality factor Q^{-1} (a) and frequency spectrum (b). Sand 3, $L = 0.1$ m, gas saturation 90 per cent.

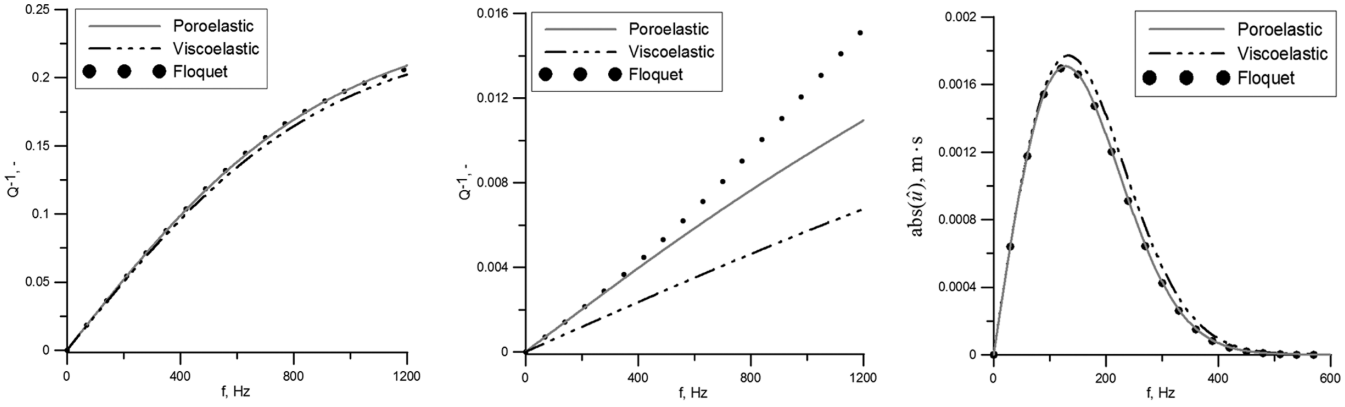

Figure 9. Inverse quality factor Q^{-1} for gas saturation 10 per cent (a) and for gas saturation 90 per cent (b); frequency spectrum for gas saturation 90 per cent (c). Sand 4, $L = 0.1$ m.

7 CONCLUSIONS

The effective viscoelastic model of White which consists of a homogeneous porous frame saturated by gas and fluid layers that are organized in a periodic way, has been the starting point of many studies in the research on wave attenuation in partially saturated media (i.e. media having gas inclusions). The model describes wave propagation in the direction normal to the layering and employs the so-called no-flow boundary condition at the outer edges of the representative elementary cell of the effective medium. In this paper we derived an effective medium for the same configuration, but employed the pressure continuity condition rather than the no-flow condition, as suggested by Dutta & Ode (1979). This choice leads to an effective poroelastic model that has two degrees of freedom, the frame and fluid displacements, and that allows the existence of both the fast and slow compressional waves. We derived frequency-dependent effective poroelastic parameters as well as their low-frequency approximations. The numerical results show that the frequency-dependent attenuation of the fast compressional wave and the transient point-source response are in agreement with the exact solution obtained using Floquet's theory, both for materials with stiff and weak frames, and for materials with high and low Biot critical frequency. For materials with weak frame, the predictions of White's model are less accurate. In the case of low Biot critical frequency White's effective viscoelastic model fails as it does not incorporate Biot's wavelength-scale attenuation mechanism. This mechanism is, however, captured by the current effective poroelastic model due to the application of the pressure continuity condition that allows relative fluid-to-solid motion at the outer edges of the representative element, and consequently on the wavelength scale. We expect that the analysis in this paper has consequences for the applicability of the other models that employ the no-flow boundary conditions, particularly for wave propagation through relatively high permeable (low Biot critical frequency) materials and materials with weak frame. For well-consolidated materials with stiff frame and with Biot critical frequency much higher than the signal frequency, the newly introduced model is in agreement with the previously introduced viscoelastic model and the exact solution.

ACKNOWLEDGEMENTS

This research has been carried out in the context of the CATO-2-program. CATO-2 is the Dutch national research program on CO_2 Capture and Storage technology (CCS). The program is financially supported by the Dutch government and the CATO-2 consortium parties. The second author has been sponsored by the Research Centre ISES (Integrated Solid Earth Science).

REFERENCES

Berryman, J.G., 1986. Elastic wave attenuation in rocks containing fluids, *Appl. Phys. Lett.,* **49,** 552–554.

Biot, M.A., 1956. Theory of propagation of elastic waves in a fluid-saturated porous solid. I. Low-frequency range, *J. acoust. Soc. Am.,* **28,** 168–178.

Braga, A.B. & Hermann, G., 1992. Floquet waves in anisotropic layered composites, *J. acoust. Soc. Am.,* **91,** 1211–1227.

Brajanovski, M., Gurevich, B. & Schoenberg, M., 2005. A model for P-wave attenuation and dispersion in a porous medium permeated by aligned fractures, *Geophys. J. Int.,* **163,** 372–384.

Carcione, J.M., 2007, *Wave Fields in Real Media: Wave Propagation in Anisotropic, Anelastic, Porous and Electromagnetic Media*. Elsevier Science Ltd.

Carcione, J.M. & Picotti, S., 2006. P-wave seismic attenuation by slow-wave diffusion: effects of inhomogeneous rock properties, *Geophysics,* **71,** O1–O8.

Carcione, J.M., Morency, C. & Santos, J.E., 2010. Computational poroelasticity—a review, *Geophysics,* **75,** A229–A243.

Carcione, J.M., Santos, J.E. & Picotti, S., 2011. Anisotropic poroelasticity and wave-induced fluid flow: harmonic finite-element simulations, *Geophys. J. Int.,* **186,** 1245–1254.

Chotiros, N.P., 1995. Biot model of sound propagation in water-saturated sand, *J. acoust. Soc. Am.,* **97,** 199–214.

Deng, J., Qu, S., Wang, S., Zhu, S. & Wang, X., 2012. P-wave attenuation and dispersion in a porous medium permeated by aligned fractures—a new poroelastic approach, *J. geophys. Eng.,* **9,** 115–126.

Deresiewicz, H. & Skalak, R., 1963. On uniqueness in dynamic poroelasticity, *Bull. seism. Soc. Am.,* **53,** 783–788.

Dutta, N.C. & Ode, H., 1979. Attenuation and dispersion of compressional waves in fluid-filled porous rocks with partial gas saturation (White model)—Part I: Biot theory, *Geophysics,* **44,** 1777–1788.

Dutta, N.C. & Seriff, A.J., 1979. On White's model of attenuation in rocks with partial gas saturation, *Geophysics,* **44,** 1806–1812.

Floquet, G., 1883. Sur les équations différentielles linéaires à coefficients périodiques. *Ann. Sci. Ec. Normale Super.,* **2,** 47–88.

Gelinsky, S. & Shapiro, S.A., 1997. Poroelastic Backus averaging for anisotropic layered fluid- and gas-saturated sediments, *Geophysics,* **62,** 1867–1878.

Gelinsky, S., Shapiro, S.A., Müller, T. & Gurevich, B., 1998. Dynamic poroelasticity of thinly layered structures, *Int. J. Solids Struct.,* **35,** 4739–4751.

Hefner, B.T. & Jackson, D.R., 2010. Dispersion and attenuation due to scattering from heterogeneities of the frame bulk modulus of a poroelastic medium *J. acoust. Soc. Am.,* **127,** 3372–3384.

Johnson, D.L., Koplik, J. & Dashen, R., 1987. Theory of dynamic permeability and tortuosity in fluid-saturated porous media, *J. Fluid Mech.,* **176,** 379–402.

Krzikalla, F. & Müller, T.M., 2011. Anisotropic P-SV-wave dispersion and attenuation due to inter-layer flow in thinly layered porous rocks, *Geophysics,* **76,** WA135–WA145.

Müller, T.M. & Gurevich, B., 2005. Wave-induced fluid flow in random porous media: attenuation and dispersion of elastic waves, *J. acoust. Soc. Am.,* **117,** 2732–2741.

Müller, T.M., Gurevich, B. & Lebedev, M., 2010. Seismic wave attenuation and dispersion resulting from wave-induced flow in porous rocks—a review, *Geophysics,* **75,** A147–A164.

Norris, A., 1993. Low-frequency dispersion and attenuation in partially saturated rocks, *J. acoust. Soc. Am.,* **94,** 359–370.

Picotti, S., Carcione, J.M., Gei, D., Rossi, G. & Santos, J.E., 2012. Seismic modeling to monitor CO_2 geological storage: the Atzbach-Schwanenstadt gas field, *J. geophys. Res.,* **117,** B06103, doi:10.1029/2011JB008540.

Pride, S.R. *et al.*, 2003. Permeability dependence of seismic amplitudes, *Leading Edge,* **22,** 518–525.

Pride, S.R., Berryman, J.G. & Harris, J.M., 2004. Seismic attenuation due to wave-induced flow, *J. geophys. Res.,* **109,** B01201, doi:10.1029/2003JB002639.

Rubino, J.G., Ravazzoli, C.L. & Santos, J.E., 2009. Equivalent viscoelastic solids for heterogeneous fluid-saturated porous rocks, *Geophysics,* **74,** N1–N13.

Rubino, J.G., Velis, D.R. & Sacchi, M.D., 2011. Numerical analysis of wave-induced fluid flow effects on seismic data: application to monitoring of CO_2 storage at the Sleipner field, *J. geophys. Res.,* **116,** B03306, doi:10.1029/2010JB007997.

Schanz, M., 2009. Poroelastodynamics: linear models, analytical solutions, and numerical methods, *Appl. Mech. Rev.,* **62,** 030803, doi:10.1115/1.3090831.

Schoemaker, F.C., 2011, Electrokinetic conversion, *PhD thesis,* Delft University of Technology, the Netherlands.

Turgut, A. & Yamamoto, T., 1990. Measurements of acoustic wave velocities and attenuation in marine sediments, *J. acoust. Soc. Am.,* **87,** 2376–2383.

Vogelaar, B. & Smeulders, D., 2007. Extension of White's layered model to the full frequency range, *Geophys. Prospect.,* **55,** 685–695.

White, J.E., Mikhaylova, N.G. & Lyakhovistkiy, F.M., 1975. Low-frequency seismic waves in fluid saturated layered rocks, *Phys. Solid Earth,* **11,** 654–659.

Williams, K.L., 2001. An effective density fluid model for acoustic propagation in sediments derived from Biot theory, *J. acoust. Soc. Am.,* **110,** 2276–2281.

APPENDIX A: MATRIX OF COEFFICIENTS

In this appendix the coefficients of the system of linear algebraic equations $\mathbf{AX} = \mathbf{B}$ that follow from the boundary conditions (13) are written out. $\mathbf{A}$ is the 8×8 matrix of the coefficients, $\mathbf{X}$ is a vector of unknown amplitudes $\hat{A}_i^{\mathrm{I,II}}$:

$$\mathbf{X} = \left[\hat{A}_1^{\mathrm{I}} \quad \hat{A}_2^{\mathrm{I}} \quad \hat{A}_3^{\mathrm{I}} \quad \hat{A}_4^{\mathrm{I}} \quad \hat{A}_1^{\mathrm{II}} \quad \hat{A}_2^{\mathrm{II}} \quad \hat{A}_3^{\mathrm{II}} \quad \hat{A}_4^{\mathrm{II}}\right]^{\mathrm{T}}. \tag{A1}$$

The amplitudes $\hat{A}_i^{\mathrm{I,II}}$ are the amplitudes of the displacements $\hat{u}_{\mathrm{I,II}}$, $\hat{w}_{\mathrm{I,II}}$

$$\hat{u}_{\mathrm{I,II}} = \hat{A}_1^{\mathrm{I,II}} \mathrm{e}^{\mathrm{i}k_{P1}^{\mathrm{I,II}} x} + \hat{A}_2^{\mathrm{I,II}} \mathrm{e}^{-\mathrm{i}k_{P1}^{\mathrm{I,II}} x} + \hat{A}_3^{\mathrm{I,II}} \mathrm{e}^{\mathrm{i}k_{P2}^{\mathrm{I,II}} x} + \hat{A}_4^{\mathrm{I,II}} \mathrm{e}^{-\mathrm{i}k_{P2}^{\mathrm{I,II}} x},$$

$$\hat{w}_{\mathrm{I,II}} = \hat{\beta}_{P1}^{\mathrm{I,II}} \hat{A}_1^{\mathrm{I,II}} \mathrm{e}^{\mathrm{i}k_{P1}^{\mathrm{I,II}} x} + \hat{\beta}_{P1}^{\mathrm{I,II}} \hat{A}_2^{\mathrm{I,II}} \mathrm{e}^{-\mathrm{i}k_{P1}^{\mathrm{I,II}} x} + \hat{\beta}_{P2}^{\mathrm{I,II}} \hat{A}_3^{\mathrm{I,II}} \mathrm{e}^{\mathrm{i}k_{P2}^{\mathrm{I,II}} x} + \hat{\beta}_{P2}^{\mathrm{I,II}} \hat{A}_4^{\mathrm{I,II}} \mathrm{e}^{-\mathrm{i}k_{P2}^{\mathrm{I,II}} x}. \tag{A2}$$

$\mathbf{B}$ is a vector containing the right-hand side of the system

$$\mathbf{B} = [\hat{\sigma} \quad \hat{p} \quad \hat{\sigma} \quad \hat{p} \quad 0 \quad 0 \quad 0 \quad 0]^{\mathrm{T}}. \tag{A3}$$

The coefficients A_{ij} of the matrix $\mathbf{A}$ read

$$A_{11} = \mathrm{i}k_{P1}^{\mathrm{I}} \left\{ Q_{\mathrm{I}} - \phi_{\mathrm{I}}(P_{\mathrm{I}} + Q_{\mathrm{I}}) + [R_{\mathrm{I}} - \phi_{\mathrm{I}}(Q_{\mathrm{I}} + R_{\mathrm{I}})] \hat{\beta}_{P1}^{\mathrm{I}} \right\} \exp\left(-\mathrm{i}k_{P1}^{\mathrm{I}} l_{\mathrm{I}}\right) / \phi_{\mathrm{I}},$$

$$A_{12} = -\mathrm{i}k_{P1}^{\mathrm{I}} \left\{ Q_{\mathrm{I}} - \phi_{\mathrm{I}}(P_{\mathrm{I}} + Q_{\mathrm{I}}) + [R_{\mathrm{I}} - \phi_{\mathrm{I}}(Q_{\mathrm{I}} + R_{\mathrm{I}})] \hat{\beta}_{P1}^{\mathrm{I}} \right\} \exp\left(\mathrm{i}k_{P1}^{\mathrm{I}} l_{\mathrm{I}}\right) / \phi_{\mathrm{I}},$$

$$
\begin{aligned}
A_{13} &= \mathrm{i}k^{\mathrm{I}}_{P2}\left\{Q_{\mathrm{I}} - \phi_{\mathrm{I}}(P_{\mathrm{I}} + Q_{\mathrm{I}}) + [R_{\mathrm{I}} - \phi_{\mathrm{I}}(Q_{\mathrm{I}} + R_{\mathrm{I}})]\hat{\beta}^{\mathrm{I}}_{P2}\right\}\exp\left(-\mathrm{i}k^{\mathrm{I}}_{P2}l_{\mathrm{I}}\right)/\phi_{\mathrm{I}},\\
A_{14} &= -\mathrm{i}k^{\mathrm{I}}_{P2}\left\{Q_{\mathrm{I}} - \phi_{\mathrm{I}}(P_{\mathrm{I}} + Q_{\mathrm{I}}) + [R_{\mathrm{I}} - \phi_{\mathrm{I}}(Q_{\mathrm{I}} + R_{\mathrm{I}})]\,\hat{\beta}^{\mathrm{I}}_{P2}\right\}\exp\left(\mathrm{i}k^{\mathrm{I}}_{P2}l_{\mathrm{I}}\right)/\phi_{\mathrm{I}},\\
A_{15} &= A_{16} = A_{17} = A_{18} = 0.
\end{aligned}
\tag{A4}
$$

$$
\begin{aligned}
A_{21} &= -\mathrm{i}k^{\mathrm{I}}_{P1}\left(Q_{\mathrm{I}} + R_{\mathrm{I}}\hat{\beta}^{\mathrm{I}}_{P1}\right)\exp\left(-\mathrm{i}k^{\mathrm{I}}_{P1}l_{\mathrm{I}}\right)/\phi_{\mathrm{I}},\\
A_{22} &= \mathrm{i}k^{\mathrm{I}}_{P1}\left(Q_{\mathrm{I}} + R_{\mathrm{I}}\hat{\beta}^{\mathrm{I}}_{P1}\right)\exp\left(\mathrm{i}k^{\mathrm{I}}_{P1}l_{\mathrm{I}}\right)/\phi_{\mathrm{I}},\\
A_{23} &= -\mathrm{i}k^{\mathrm{I}}_{P2}\left(Q_{\mathrm{I}} + R_{\mathrm{I}}\hat{\beta}^{\mathrm{I}}_{P2}\right)\exp\left(-\mathrm{i}k^{\mathrm{I}}_{P2}l_{\mathrm{I}}\right)/\phi_{\mathrm{I}},\\
A_{24} &= \mathrm{i}k^{\mathrm{I}}_{P2}\left(Q_{\mathrm{I}} + R_{\mathrm{I}}\hat{\beta}^{\mathrm{I}}_{P2}\right)\exp\left(\mathrm{i}k^{\mathrm{I}}_{P2}l_{\mathrm{I}}\right)/\phi_{\mathrm{I}},\\
A_{25} &= A_{26} = A_{27} = A_{28} = 0.
\end{aligned}
\tag{A5}
$$

$$
\begin{aligned}
A_{31} &= A_{32} = A_{33} = A_{34} = 0,\\
A_{35} &= \mathrm{i}k^{\mathrm{II}}_{P1}\left\{Q_{\mathrm{II}} - \phi_{\mathrm{II}}(P_{\mathrm{II}} + Q_{\mathrm{II}}) + [R_{\mathrm{II}} - \phi_{\mathrm{II}}(Q_{\mathrm{II}} + R_{\mathrm{II}})]\,\hat{\beta}^{\mathrm{II}}_{P1}\right\}\exp\left(\mathrm{i}k^{\mathrm{II}}_{P1}l_{\mathrm{II}}\right)/\phi_{\mathrm{II}},\\
A_{36} &= -\mathrm{i}k^{\mathrm{II}}_{P1}\left\{Q_{\mathrm{II}} - \phi_{\mathrm{II}}(P_{\mathrm{II}} + Q_{\mathrm{II}}) + [R_{\mathrm{II}} - \phi_{\mathrm{II}}(Q_{\mathrm{II}} + R_{\mathrm{II}})]\,\hat{\beta}^{\mathrm{II}}_{P1}\right\}\exp\left(-\mathrm{i}k^{\mathrm{II}}_{P1}l_{\mathrm{II}}\right)/\phi_{\mathrm{II}},\\
A_{37} &= \mathrm{i}k^{\mathrm{II}}_{P2}\left\{Q_{\mathrm{II}} - \phi_{\mathrm{II}}(P_{\mathrm{II}} + Q_{\mathrm{II}}) + [R_{\mathrm{II}} - \phi_{\mathrm{II}}(Q_{\mathrm{II}} + R_{\mathrm{II}})]\,\hat{\beta}^{\mathrm{II}}_{P2}\right\}\exp\left(\mathrm{i}k^{\mathrm{II}}_{P2}l_{\mathrm{II}}\right)/\phi_{\mathrm{II}},\\
A_{38} &= -\mathrm{i}k^{\mathrm{II}}_{P2}\left\{Q_{\mathrm{II}} - \phi_{\mathrm{II}}(P_{\mathrm{II}} + Q_{\mathrm{II}}) + [R_{\mathrm{II}} - \phi_{\mathrm{II}}(Q_{\mathrm{II}} + R_{\mathrm{II}})]\,\hat{\beta}^{\mathrm{II}}_{P2}\right\}\exp\left(-\mathrm{i}k^{\mathrm{II}}_{P2}l_{\mathrm{II}}\right)/\phi_{\mathrm{II}}.
\end{aligned}
\tag{A6}
$$

$$
\begin{aligned}
A_{41} &= A_{42} = A_{43} = A_{44} = 0,\\
A_{45} &= -\mathrm{i}k^{\mathrm{II}}_{P1}\left(Q_{\mathrm{II}} + R_{\mathrm{II}}\hat{\beta}^{\mathrm{II}}_{P1}\right)\exp\left(\mathrm{i}k^{\mathrm{II}}_{P1}l_{\mathrm{II}}\right)/\phi_{\mathrm{II}},\\
A_{46} &= \mathrm{i}k^{\mathrm{II}}_{P1}\left(Q_{\mathrm{II}} + R_{\mathrm{II}}\hat{\beta}^{\mathrm{II}}_{P1}\right)\exp\left(-\mathrm{i}k^{\mathrm{II}}_{P1}l_{\mathrm{II}}\right)/\phi_{\mathrm{II}},\\
A_{47} &= -\mathrm{i}k^{\mathrm{II}}_{P2}\left(Q_{\mathrm{II}} + R_{\mathrm{II}}\hat{\beta}^{\mathrm{II}}_{P2}\right)\exp\left(\mathrm{i}k^{\mathrm{II}}_{P2}l_{\mathrm{II}}\right)/\phi_{\mathrm{II}},\\
A_{48} &= \mathrm{i}k^{\mathrm{II}}_{P2}\left(Q_{\mathrm{II}} + R_{\mathrm{II}}\hat{\beta}^{\mathrm{II}}_{P2}\right)\exp\left(-\mathrm{i}k^{\mathrm{II}}_{P2}l_{\mathrm{II}}\right)/\phi_{\mathrm{II}}.
\end{aligned}
\tag{A7}
$$

$$
\begin{aligned}
A_{51} &= A_{52} = \phi_{\mathrm{I}}\left(1 - \hat{\beta}^{\mathrm{I}}_{P1}\right),\\
A_{53} &= A_{54} = \phi_{\mathrm{I}}\left(1 - \hat{\beta}^{\mathrm{I}}_{P2}\right),\\
A_{55} &= A_{56} = -\phi_{\mathrm{II}}\left(1 - \hat{\beta}^{\mathrm{II}}_{P1}\right),\\
A_{57} &= A_{58} = -\phi_{\mathrm{II}}\left(1 - \hat{\beta}^{\mathrm{II}}_{P2}\right).
\end{aligned}
\tag{A8}
$$

$$
\begin{aligned}
A_{61} &= A_{62} = A_{63} = A_{64} = 1,\\
A_{65} &= A_{66} = A_{67} = A_{68} = -1.
\end{aligned}
\tag{A9}
$$

$$
\begin{aligned}
A_{71} &= -A_{72} = -\mathrm{i}k^{\mathrm{I}}_{P1}\left(Q_{\mathrm{I}} + R_{\mathrm{I}}\hat{\beta}^{\mathrm{I}}_{P1}\right)/\phi_{\mathrm{I}},\\
A_{73} &= -A_{74} = -\mathrm{i}k^{\mathrm{I}}_{P2}\left(Q_{\mathrm{I}} + R_{\mathrm{I}}\hat{\beta}^{\mathrm{I}}_{P2}\right)/\phi_{\mathrm{I}},\\
A_{75} &= -A_{76} = \mathrm{i}k^{\mathrm{II}}_{P1}\left(Q_{\mathrm{II}} + R_{\mathrm{II}}\hat{\beta}^{\mathrm{II}}_{P1}\right)/\phi_{\mathrm{II}},\\
A_{77} &= -A_{78} = \mathrm{i}k^{\mathrm{II}}_{P2}\left(Q_{\mathrm{II}} + R_{\mathrm{II}}\hat{\beta}^{\mathrm{II}}_{P2}\right)/\phi_{\mathrm{II}}.
\end{aligned}
\tag{A10}
$$

$$
\begin{aligned}
A_{81} &= -A_{82} = \mathrm{i}k^{\mathrm{I}}_{P1}\left\{Q_{\mathrm{I}} - \phi_{\mathrm{I}}(P_{\mathrm{I}} + Q_{\mathrm{I}}) + [R_{\mathrm{I}} - \phi_{\mathrm{I}}(Q_{\mathrm{I}} + R_{\mathrm{I}})]\hat{\beta}^{\mathrm{I}}_{P1}\right\},\\
A_{83} &= -A_{84} = \mathrm{i}k^{\mathrm{I}}_{P2}\left\{Q_{\mathrm{I}} - \phi_{\mathrm{I}}(P_{\mathrm{I}} + Q_{\mathrm{I}}) + [R_{\mathrm{I}} - \phi_{\mathrm{I}}(Q_{\mathrm{I}} + R_{\mathrm{I}})]\hat{\beta}^{\mathrm{I}}_{P2}\right\},\\
A_{85} &= -A_{86} = -\mathrm{i}k^{\mathrm{II}}_{P1}\left\{Q_{\mathrm{II}} - \phi_{\mathrm{II}}(P_{\mathrm{II}} + Q_{\mathrm{II}}) + [R_{\mathrm{II}} - \phi_{\mathrm{II}}(Q_{\mathrm{II}} + R_{\mathrm{II}})]\hat{\beta}^{\mathrm{II}}_{P1}\right\},\\
A_{87} &= -A_{88} = -\mathrm{i}k^{\mathrm{II}}_{P2}\left\{Q_{\mathrm{II}} - \phi_{\mathrm{II}}(P_{\mathrm{II}} + Q_{\mathrm{II}}) + [R_{\mathrm{II}} - \phi_{\mathrm{II}}(Q_{\mathrm{II}} + R_{\mathrm{II}})]\hat{\beta}^{\mathrm{II}}_{P2}\right\}.
\end{aligned}
\tag{A11}
$$

APPENDIX B: LOW-FREQUENCY APPROXIMATION OF THE EFFECTIVE COEFFICIENTS

In this Appendix a perturbation approach is presented which is used to derive the low-frequency approximations (18) of the effective coefficients (17). For this purpose, the displacement fields are expanded in the Taylor series

$$\hat{u} = u_0 + \omega u_1 + \omega^2 u_2 + \mathcal{O}(\omega^3),$$
$$\hat{w} = w_0 + \omega w_1 + \omega^2 w_2 + \mathcal{O}(\omega^3). \tag{B1}$$

The viscodynamic operator $\hat{b}$ contained in the density terms $\hat{\rho}_{ij}$ is also expanded in a series of ω

$$\hat{b} = b_0\sqrt{1 + \mathrm{i}\frac{\omega}{2\omega_\mathrm{B}}} = b_0\left[1 + \frac{\mathrm{i}\omega}{4\omega_\mathrm{B}} + \frac{\omega^2}{32\omega_\mathrm{B}^2} + \mathcal{O}(\omega^3)\right]. \tag{B2}$$

These expansions are substituted into Biot's equations in the frequency domain. Then the equations are solved for each power of ω with the boundary conditions (13). The strains of the elementary cell are found as linear combinations of $\hat{\sigma}$ and $\hat{p}$, as before (eq. 16), but now the analytical expressions for the low-frequency terms of the coefficients α_1 to α_4 can be obtained

$$\frac{\hat{u}(l_\mathrm{II}) - \hat{u}(-l_\mathrm{I})}{L} = (a_{10} + \omega a_{11} + \omega^2 a_{12} + \cdots)\hat{\sigma} + (a_{20} + \omega a_{21} + \omega^2 a_{22} + \cdots)\hat{p},$$
$$\frac{\hat{w}(l_\mathrm{II}) - \hat{w}(-l_\mathrm{I})}{L} = (a_{20} + \omega a_{21} + \omega^2 a_{22} + \cdots)\hat{\sigma} + (a_{40} + \omega a_{41} + \omega^2 a_{42} + \cdots)\hat{p}. \tag{B3}$$

All the coefficients a_{ij} are independent of frequency, but do depend on the properties of both layers, and can be found analytically. Then the terms of the expansions of the effective coefficients (eq. 18) can be obtained analytically as combinations of the coefficients a_{ij}. The explicit expressions are not presented here for reasons of brevity. They can be derived with the use of any symbolic software.

APPENDIX C: FLOQUET SOLUTION

In this appendix the exact solution for a periodically layered porous half-space with excitation at the top (Fig. 2a) is derived by the use of Floquet's theory (Floquet 1883). The derivation is similar to that given in Braga & Hermann (1992) for an elastic layered composite.

The equations of motion and stress–strain relations (1)–(3) can be rewritten in the space-frequency domain into a linear differential equation of the first order in the following matrix form:

$$\frac{\partial\hat{\mathbf{f}}(x)}{\partial x} = \mathrm{i}\hat{\mathbf{N}}(x)\hat{\mathbf{f}}(x), \tag{C1}$$

where $\hat{\mathbf{f}} = [\mathrm{i}\omega\hat{u}, \mathrm{i}\omega\hat{\zeta}, \hat{\sigma}, \hat{p}]$ is a vector containing field variables, namely, solid particle velocity, relative velocity, intergranular stress and pore pressure. All the elements of this vector are continuous at the interfaces between the layers (Deresiewicz & Skalak 1963). $\hat{\mathbf{N}}$ is a 4×4 matrix of coefficients that describe the material properties

$$\hat{\mathbf{N}} = \begin{bmatrix} \mathbf{0} & \mathbf{N}^a \\ \hat{\mathbf{N}}^b & \mathbf{0} \end{bmatrix},$$
$$\mathbf{N}^a = \frac{1}{PR - Q^2}\begin{bmatrix} -R & \phi(R+Q) - R \\ \phi(Q+R) & \phi(Q+R) - \phi^2(P+2Q+R) \end{bmatrix},$$
$$\hat{\mathbf{N}}^b = \frac{\omega^2}{\phi}\begin{bmatrix} \hat{\rho}_{12}(1-2\phi) + \hat{\rho}_{22}(1-\phi) - \phi\hat{\rho}_{11} & (\hat{\rho}_{22}(1-\phi) - \phi\hat{\rho}_{12})/\phi \\ -(\hat{\rho}_{12} + \hat{\rho}_{22}) & -\hat{\rho}_{22}/\phi \end{bmatrix}. \tag{C2}$$

The elements of the matrix $\hat{\mathbf{N}}$ are piecewise constant functions of the coordinate x, they are constant inside each layer and periodic with the period $L = l_\mathrm{I} + l_\mathrm{II}$. Thus, eq. (C1) is a system of four linear differential equations with a periodic matrix of coefficients. Its solution can be expressed via the fundamental matrix of solutions $\hat{\mathbf{X}}$

$$\hat{\mathbf{f}}(x) = \hat{\mathbf{X}}(x)\mathbf{c}, \tag{C3}$$

where $\mathbf{c}$ is a column of constants to be found from the boundary conditions. According to Floquet's theory, the matrix $\hat{\mathbf{X}}(x)$ can be found in the form

$$\hat{\mathbf{X}}(x) = \hat{\mathbf{F}}(x)\exp(\mathrm{i}\hat{\mathbf{A}}x), \tag{C4}$$

where $\hat{\mathbf{F}}(x + L) = \hat{\mathbf{F}}(x)$ is a yet unknown periodic matrix and matrix $\hat{\mathbf{A}}$ is constant (with respect to x).

First, the matrix $\hat{\mathbf{A}}$ has to be found. In each of the layers $k = 1, 2$ the solution of eq. (C1) is

$$\hat{\mathbf{f}}_k(x) = \hat{\mathbf{M}}_k(x)\hat{\mathbf{f}}_k(0), \tag{C5}$$

where $\hat{\mathbf{M}}_k(x) = \exp(\mathrm{i}\hat{\mathbf{N}}_k x)$ and $\hat{\mathbf{M}}_k(0) = \mathbf{I}$, where $\mathbf{I}$ is the identity matrix. By analogy, the solution of eq. (C1) for the stack of periodic layers can be expressed in the same manner

$$\hat{\mathbf{f}}(x) = \hat{\mathbf{P}}(x)\hat{\mathbf{f}}(0). \tag{C6}$$

It follows from (C6) that $\hat{\mathbf{P}}(0) = \mathbf{I}$. The solution $\hat{\mathbf{f}}(x)$ can be also expressed via the fundamental matrix (C4) as

$$\hat{\mathbf{f}}(x) = \hat{\mathbf{F}}(x)\exp(\mathrm{i}\hat{\mathbf{A}}x)\hat{\mathbf{f}}(0). \tag{C7}$$

Then, the periodic matrix $\hat{\mathbf{F}}(L) = \hat{\mathbf{F}}(0) = \mathbf{I}$ and $\hat{\mathbf{P}}(L) = \exp(\mathrm{i}\hat{\mathbf{A}}L)$. On the other hand, using (C5), the vector $\hat{\mathbf{f}}(L)$ can be expressed as

$$\hat{\mathbf{f}}(L) = \hat{\mathbf{M}}_2(l_{\mathrm{II}})\hat{\mathbf{M}}_1(l_{\mathrm{I}})\hat{\mathbf{f}}(0). \tag{C8}$$

Thus, the matrix $\hat{\mathbf{A}}$ can be found from the following exponential relations:

$$\hat{\mathbf{P}}(L) = \exp(\mathrm{i}\hat{\mathbf{A}}L) = \exp(\mathrm{i}\hat{\mathbf{N}}_2 l_{\mathrm{II}})\exp(\mathrm{i}\hat{\mathbf{N}}_1 l_{\mathrm{I}}). \tag{C9}$$

The eigenvalues k_i^F of the matrix $\hat{\mathbf{A}}$ are the so-called Floquet wavenumbers. They are exponentially related to the eigenvalues τ_i of the matrix $\exp(\mathrm{i}\hat{\mathbf{A}}L)$: $\tau_i = \exp(\mathrm{i}k_i^F L)$.

Next, the periodic function $\hat{\mathbf{F}}(x)$ is determined. First, the local coordinate x_n is introduced

$$x_n = x - (n-1)L, \qquad 0 \le x_n \le L, \qquad n = 1, 2, \ldots \tag{C10}$$

The following equalities hold true (*cf.* C6 and C7):

$$\hat{\mathbf{P}}(x) = \hat{\mathbf{F}}(x)\exp(\mathrm{i}\hat{\mathbf{A}}x) = \hat{\mathbf{F}}(x_n)\exp(\mathrm{i}\hat{\mathbf{A}}x_n)\exp[\mathrm{i}\hat{\mathbf{A}}L(n-1)] = \hat{\mathbf{P}}(x_n)\exp[\mathrm{i}\hat{\mathbf{A}}L(n-1)]. \tag{C11}$$

After right-multiplying (C11) by $\exp(-\mathrm{i}\mathbf{A}x)$ one recognizes

$$\hat{\mathbf{F}}(x) = \hat{\mathbf{P}}(x_n)\exp(-\mathrm{i}\hat{\mathbf{A}}x_n). \tag{C12}$$

The matrix $\hat{\mathbf{P}}(x_n)$ is the propagator matrix at a distance x_n from the interface between the unit cells $(n-1)$ and n. From (C5) and (C6) it can be concluded that

$$\hat{\mathbf{P}}(x_n) = \begin{cases} \hat{\mathbf{M}}_1(x_n), & 0 \le x_n \le l_I; \\ \hat{\mathbf{M}}_2(x_n - l_1)\hat{\mathbf{M}}_1(l_1), & l_I \le x_n \le L. \end{cases} \tag{C13}$$

Hence, the periodic matrix $\hat{\mathbf{F}}(x)$ is determined.

Finally, the solution for a periodically layered system, with a unit cell consisting of two layers, is found in the space-frequency domain. By combining (C7), (C10) and (C12) the solution $\hat{\mathbf{f}}(x)$ is expressed in the following way:

$$\hat{\mathbf{f}}(x) = \hat{\mathbf{F}}(x)\exp(\mathrm{i}\hat{\mathbf{A}}x)\hat{\mathbf{f}}(0) = \hat{\mathbf{P}}(x_n)\exp[\mathrm{i}\hat{\mathbf{A}}L(n-1)]\hat{\mathbf{f}}(0). \tag{C14}$$

The next step towards the calculation of the field variables contained in $\hat{\mathbf{f}}$ is to find the four unknowns $\hat{\mathbf{f}}(0)$. The displacement field in the first layer $0 \le x \le l_{\mathrm{I}}$ is simply a solution of Biot's equations (11). Then the vector $\hat{\mathbf{f}}(0)$ can be expressed as a product of a matrix of coefficients and a column of unknown amplitudes $\hat{A}_1$ to $\hat{A}_4$

$$\hat{\mathbf{f}}(0) = \begin{bmatrix} \mathrm{i}\omega & \mathrm{i}\omega & \mathrm{i}\omega & \mathrm{i}\omega \\ \mathrm{i}\omega\phi_{\mathrm{I}}\left(\hat{\beta}^{\mathrm{I}}_{P1} - 1\right) & \mathrm{i}\omega\phi_{\mathrm{I}}\left(\hat{\beta}^{\mathrm{I}}_{P2} - 1\right) & \mathrm{i}\omega\phi_{\mathrm{I}}\left(\hat{\beta}^{\mathrm{I}}_{P1} - 1\right) & \mathrm{i}\omega\phi_{\mathrm{I}}\left(\hat{\beta}^{\mathrm{I}}_{P2} - 1\right) \\ g_{P1} & g_{P2} & -g_{P1} & -g_{P2} \\ h_{P1} & h_{P2} & -h_{P1} & -h_{P2} \end{bmatrix} \begin{bmatrix} \hat{A}_1 \\ \hat{A}_2 \\ \hat{A}_3 \\ \hat{A}_4 \end{bmatrix}, \tag{C15}$$

where

$$g_{P1,P2} = \frac{-\mathrm{i}k^{\mathrm{I}}_{P1,P2}}{\phi_{\mathrm{I}}}\left[\phi_{\mathrm{I}}P_{\mathrm{I}} - Q_{\mathrm{I}} + \phi_{\mathrm{I}}Q_{\mathrm{I}} + \hat{\beta}^{\mathrm{I}}_{P1,P2}(\phi_{\mathrm{I}}R_{\mathrm{I}} + \phi_{\mathrm{I}}Q_{\mathrm{I}} - R_{\mathrm{I}})\right],$$

$$h_{P1,P2} = \frac{-\mathrm{i}k^{I}_{P1,P2}}{\phi_{\mathrm{I}}}\left(Q_{\mathrm{I}} + \hat{\beta}^{\mathrm{I}}_{P1,P2}R_{\mathrm{I}}\right). \tag{C16}$$

There are four equations to determine the four complex-valued amplitudes $\hat{A}_i$. The first two equations come from the boundary conditions at the top interface (22) that assign the values for the third and the fourth components of the vector $\hat{\mathbf{f}}$. The second two come from the elimination of the upgoing Floquet waves in the solution (C14): as there are no sources of energy at any place below the top of the half-space $x = 0$, the field variables (like displacements) should tend to zero when $x \to \infty$ (not to some finite value due to the presence of viscous damping in the system). Thus, the coefficients of the exponential terms in (C14) that correspond to the upgoing Floquet waves (there are two of them, the slow and the fast *P*-waves) should be zeros, and these conditions provide another two equations to solve for the unknown amplitudes.